JOURNAL OF MATERIALS SCIENCE 30 (1995) 5777–5783

Characterization of Na–X, Na–A, and coal fly ash zeolites and their amorphous precursors by IR, MAS NMR and XPS

N. SHIGEMOTO, S. SUGIYAMA, H. HAYASHI
Department of Chemical Science and Technology, University of Tokushima; 2-1 Minamijosanjima 770 Japan

K. MIYAURA
Shikoku Research Institute Inc., 2109 Yashima-nishimachi Takamatsu, 761-01 Japan

By fusion with sodium hydroxide followed by a hydrothermal reaction, fly ash and Al-enriched fly ash were converted into Na–X and Na–A zeolites, respectively. The authentic Na–X, Na–A and fly ash zeolites as well as their amorphous precursors have been characterized by IR, ^{29}Si and ^{27}Al MAS NMR, XPS/AES, TG, and comparative ion-exchange studies of Cs and K with Na in zeolite samples. It appears that the same structural unit with a terminal OH, such as a sodalite unit, was formed in the induction period of the hydrothermal reaction for Na–X and Na–A, and then cross-linked through D4R and D6R external linkages to build up the zeolite framework of Na–A and Na–X, respectively.

1. Introduction

Coal fly ash, which is formed as a waste by-product at coal-fired power plants, is an agglomerate of spheres or cenospheres of 1–100 μm in diameter and contains silicon and aluminium as the major elements [1, 2].

Hydrothermal treatment of coal fly ash with a sodium hydroxide solution at 373 K under vigorous agitation gives various types of zeolites such as Na–P1, Na–A and hydroxysodalite, where a zeolite zone is formed like an egg-white covering the central core of fly ash particles [3]. By fusion with sodium hydroxide followed by the hydrothermal reaction at 373 K without stirring, fly ash and aluminium-enriched fly ash were favourably converted into Na–X and Na–A zeolite, respectively [4]. In these hydrothermal reactions, zeolites were abruptly crystallized after an induction period, from amorphous aluminosilicate gels which existed during the induction period [5].

In the present work, Na–X, Na–A, and fly ash zeolites and their amorphous precursors have been characterized in order to elucidate the crystallization processes by following analytical methods: infrared spectroscopy (IR), magic angle spinning nuclear magnetic resonance (MAS NMR), X-ray photoelectron (XPS) and Auger electron (AES) spectroscopy and thermogravimetric (TG) analysis.

Comparative ion-exchange studies of Cs and K with Na–X are also described, providing evidence for the formation of zeolite frameworks by double six-membered ring (D6R) linkages of sodalite units.

2. Experimental procedure

2.1. Zeolite synthesis

Hydrothermal reactions for Na–X [6] and Na–A [7] zeolite synthesis from pure reagents were carried out as follows. A clear solution of sodium aluminate in sodium hydroxide was mixed with an aqueous solution of sodium silicate in an appropriate ratio to adjust the starting composition to 7.38 $Na_2O \cdot Al_2O_3 \cdot 5.03\ SiO_2 \cdot 400\ H_2O$ for Na–X [6] and 3.42 $Na_2O \cdot Al_2O_3 \cdot 2.00\ SiO_2 \cdot 200\ H_2O$ for Na–A [7], respectively. A slurry thus formed as agitated magnetically for 18 h at room temperature, and each 10 ml of the slurry was heated at 373 K in a sealed Teflon tube for a given period. The solid phase was filtered, repeatedly washed with water, and dried overnight at 373 K.

Procedures for zeolite synthesis from fly ash have been described elsewhere [4].

2.2. Reagents

Sodium metasilicate hydrate (Na_2O 19.3%, SiO_2 21.5%, H_2O 58.0%) and sodium hydroxide (>99%) were purchased from Wako Pure Chemical Industries, Ltd, Osaka, and were used as supplied. Sodium aluminate (Na_2O 35.5%, Al_2O_3 34.8%) obtained from Wako was dissolved in water, and the aqueous solution was boiled, cooled to room temperature, and filtered to remove the small amounts of impurities such as iron hydroxide and suspended solids.

0022–2461

2.3. Analysis

IR spectra in the range of 1500 ~ 250 cm^{-1} were measured for samples pelletized with CsI with a Hitachi 270-50 spectrometer.

X-ray photoelectron and Auger spectra (AES) for Si and Al were measured with an Ulvac-Phi 5500 apparatus irradiated with MgK_α, and the results were compared on a chemical state plot: two-dimensional correlation of photoelectron binding energies (2p) and Auger kinetic energies (KLL). The observed binding and kinetic energies were calibrated with 284.6 eV [8] for C 1s electron.

The ^{29}Si and ^{27}Al NMR spectra were obtained at 53.67 and 70.40 MHz on a Hitachi R-3000 FT-NMR spectrometer employing magic angle spinning at 6 kHz. ^{29}Si and ^{27}Al chemical shifts (in ppm) were referenced to external standards of 1 M $AlCl_3$ aqueous solution ($Al(H_2O)_6^{3+}$) and tetramethylsilane (TMS), respectively.

Powder X-ray diffraction (XRD) patterns were measured using CuK_α radiation by the MXP system of MAC Science Co., Tokyo. Crystallinity of zeolite samples was defined [4] as the X-ray intensity ratio to well-crystallized zeolites at given diffraction faces of Na–A (2 0 0) and Na–X (1 1 1).

TG was performed using a TG/DTA 30 analyser of Seiko Instruments Inc., Tokyo, where samples were exposed overnight to moist air at 298 K in a desiccator.

Ion-exchange of Cs and K with Na–X carried out by the immersion of zeolite samples in 0.1 M CsCl or 0.1 M KCl solution under vigorous vibration for 4 days at 298 K. Concentrations of Na and Cs or K in liquid were determined by a Perkin-Elmer 5000 atomic absorption spectrometer. Analysis for solid phases was also made after decomposition of the zeolite sample with 1 M HCl.

The chemical compositions of zeolite samples were determined by an inductively coupled plasma atomic emission spectrometer (SPS-1500, Seiko Instruments Inc., Tokyo) after decomposition with 1 M HCl.

3. Results and discussion

3.1. Formation of zeolites under hydrothermal conditions

Fig. 1 shows crystallinity and composition of products during the hydrothermal reaction by the established procedure for authentic Na–A [7] and Na–X [6]. The crystallinity of both Na–A (Fig. 1a) and Na–X (Fig. 1b) increased abruptly after 1 h and *c.* 4 h of the induction period, respectively, followed by an increase to almost 100% crystallinity as indicated by sigmoid curve (Fig. 1b) becoming a plateau as 100% crystallinity was approached. In contrast, the molar ratio of Si/Al and Na/Al in solid phase products changed rather slightly in both series of run (Fig. 1a and b) irrespective of the abrupt increase in crystallinity, suggesting that a precursor with the composition close to the target zeolite had already formed in the induction period. Thus the amorphous solid products in the hydrothermal reaction at 1 h for Na–A and at 2 h for

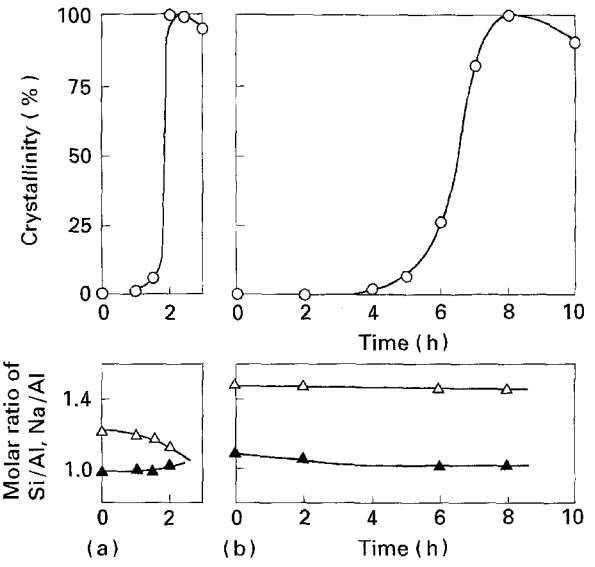

Figure 1 Transition of zeolite crystallinity and composition in hydrothermal reaction for Na–A (a) and Na–X (b); ○, crystallinity; △, Si/Al; ▲, Na/Al.

Na–X were taken in the present work as samples for amorphous precursors to compare with the well-crystallized zeolite samples. The hydrothermal reaction product with intermediate crystallinity was not used for characterization, because the product should have properties of a mixture of large zeolite crystals and amorphous compounds [5].

3.2. IR evidence for linkage of sodalite unit to build up zeolite framework

3.2.1. IR spectra and assignment for Na–X, Na–A zeolite and their amorphous precursors

Fig. 2 compares IR spectra of Na–X (curve b), Na–A (curve d) zeolite and their amorphous precursors (curves a and c). Na–A zeolite is composed of a molar ratio of Si/Al = 1, and the assignment of IR bands (Fig. 2, curve d) is rather straightforward [9]: asymmetric stretching (1016 cm^{-1}) and bending vibration (471 cm^{-1}) of T–O bond (where T = Si or Al) in TO_4 tetrahedra, and double four-membered rings (D4R, 562 cm^{-1}) and pore opening (382 cm^{-1}) of external linkages, respectively.

In contrast with Na–A, faujasite zeolites Na–X and Na–Y with various Si/Al ratios are known to exist. Fig. 3 shows a linear decrease in frequency of IR band with an increase in Al content in the faujasite zeolite [9] for each asymmetric stretching (curve a), symmetric stretching (curves b_1 and b_2), D6R (curve c), bending of T–O bond (curve d), and pore opening (curve e). It is of interest to note that the absorption band of curves a, b_2 and d in Fig. 3 were extrapolated to zero Al content in good agreement with values observed for SiO_2 gel [10, 11]. The composition of the well-crystallized Na–X zeolite prepared in the present work was Si/Al = 1.45, i.e. Al/(Al + Si) = 0.41, as given in Fig. 1b (white triangle at 8 h). The bands observed for the Na–X zeolite were plotted in Fig. 3 as white squares in good agreement with Fig. 3, curves a to e, and thus

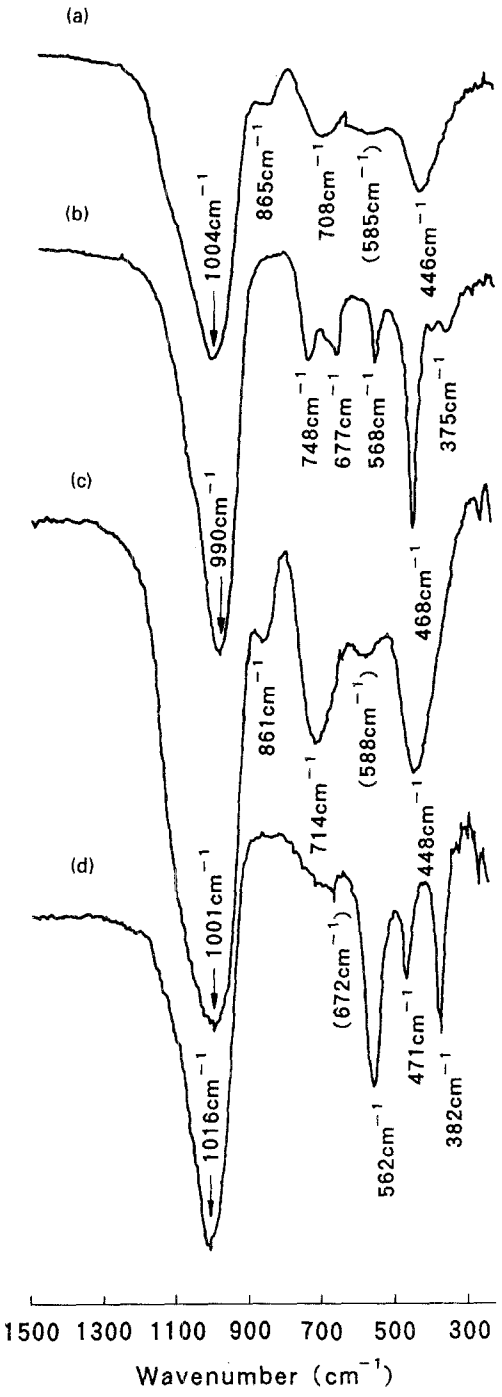

Figure 2 IR spectra for Na–X (b), Na–A zeolite (d) and their amorphous precursors ((a) for Na–X, (c) for Na–A).

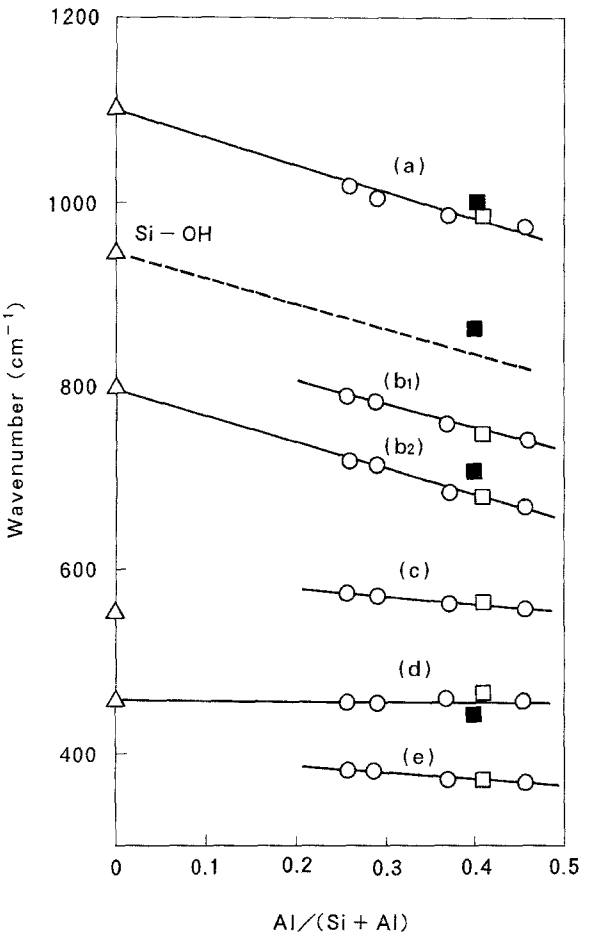

Figure 3 Shift of IR bands for faujasite zeolite with Al content in zeolite framework; ○, faujasites [9]; △, SiO_2 gel [10]; □, Na–X (present work); ■, precursor for Na–X (present work).

assigned to asymmetric stretching (990 cm^{-1}), symmetric stretching (748 cm^{-1}, 677 cm^{-1}), bending vibration (468 cm^{-1}) of T–O bond, D6R (568 cm^{-1}) and pore opening (375 cm^{-1}), respectively.

The spectrum of the amorphous precursor (Fig. 2, curve a) for Na–X was rather simple and broad as compared with that of crystalline Na–X (Fig. 2, curve b), and three bands at 1004, 708 and 446 cm^{-1} shown as black squares in Fig. 3, should be assigned to asymmetric stretching (curve a), symmetric stretching (curve b_2) and bending vibration (curve d), respectively.

A shoulder at 865 cm^{-1} (Fig. 2, curve a) observed in the amorphous precursor for Na–X presumably due to vibration of T–OH, because of a broken straight line drawn in parallel with Fig. 3, curves a and b, is reasonably extrapolated to the silanol Si–OH [10] at 950 cm^{-1}. Furthermore, in both precursors for Na–X and Na–A, the bands at *c.* 870 cm^{-1} disappeared on heating the samples at 723 K for 1 h, similar to SiO_2 gel [10, 11], signifying the presence of T–OH bond in the precursors. Stojkovic and Adnadjevic [12] have recorded IR spectra for sodium aluminosilicate gels of not yet crystallized Na–A zeolite, similar to Fig. 2, curve c, whereas a distinct band was not recognized at *c.* 870 cm^{-1}, presumably because T–OH bond disappeared before IR measurement as the samples were dried at a high temperature of 383 K.

The difference in structure between Na–X and Na–A is essentially the difference in the mode of linkage of the sodalite unit in building up the zeolite framework. Thus the spectra of amorphous precursors for Na–A (Fig. 2, curve c) and Na–X (Fig. 2, curve a) were similar as anticipated, and the bands observed for Na–A precursor could be assigned as above.

3.2.2. Linkage of sodalite unit

The bands at 568 and 375 cm^{-1} (Fig. 2b), and at 562 and 382 cm^{-1} (Fig. 2, curve d), which were absent in amorphous species (Fig. 2, curves a and c), appeared in crystalline Na–X and Na–A, respectively, and were consistent with the assignments to double ring linkages (D6R for Na–X, D4R for Na–A) and pore

opening. In contrast, the terminal T–OH bond was present in both precursors but not in the crystallized zeolites of both Na–X and Na–A.

Differences and similarities in IR spectra among zeolites and their amorphous precursors can be interpreted as that for the same structural unit with terminal T–OH, for example like a sodalite unit, being formed during the induction period of the hydrothermal reaction, and then coupling together through dehydration of the terminal OH, leading to either D6R or D4R linkages, and finally building up the crystalline zeolite framework of Na–X or Na–A, respectively.

3.2.3. Fly ash zeolites

Na–X and Na–A zeolite were formed from coal fly ash and Al-enriched fly ash, respectively, by fusion with sodium hydroxide and the succeeding hydrothermal treatment at 373 K after an induction period [4]. The IR spectra for fly ash zeolite and their amorphous intermediates were quite similar to that for corresponding authentic zeolite Na–X, Na–A and their precursors, respectively.

3.3. Cs ion exchange behaviour of Na–X zeolite and the amorphous precursor

A faujasite-type zeolite such as Na–X and Na–Y involves D6R linkages in the structural framework. It is well known that Na ions in the D6R hexagonal prism can be exchanged by small ions such as Li and K but not by large ions such as Cs and Rb [13–15]. Thus the difference in K and Cs uptake in the comparative ion-exchange, if observed, would provide evidence for the presence of the D6R linkages in a zeolite sample.

Fig. 4 compares Na–K (triangles) and Na–Cs (circles) ion-exchange isotherms at 298 K for Na–X zeolite (Fig. 4b) and for the precursor (Fig. 4a). Fig. 4b shows that all of the Na ions in the Na–X zeolite could be exchanged by K ions but only 65% of Na ions, which was extrapolated to 100% in abscissa of Na–Cs isotherm (circles in Fig. 4b), could be replaced by Cs ions in good agreement with the literature [15]. On the other hand, complete replacement of Na ions was accomplished for Na–X precursor by either K or Cs ions, as shown in Fig. 4a.

Comparative Cs/K ion-exchange behaviour obtained above signifies the D6R linkages for well-crystallized Na–X zeolite. It is of interest that the hydrothermal reaction product for Na–X includes exchangeable Na ions regardless of crystallinity of the zeolite.

3.4. TG of zeolites

Fig. 5 compares the TG curves for Na–X (b), Na–A (d) and their amorphous precursors (a and c) after saturated with moist air at room temperature. Solid lines and broken lines show samples dried at 373 and 723 K prior to exposure to moisture, respectively.

The TG curves for well-crystallized zeolites (Fig. 5b and d) show reproducible weight loss irrespective of the preheating temperature: solid and broken lines are

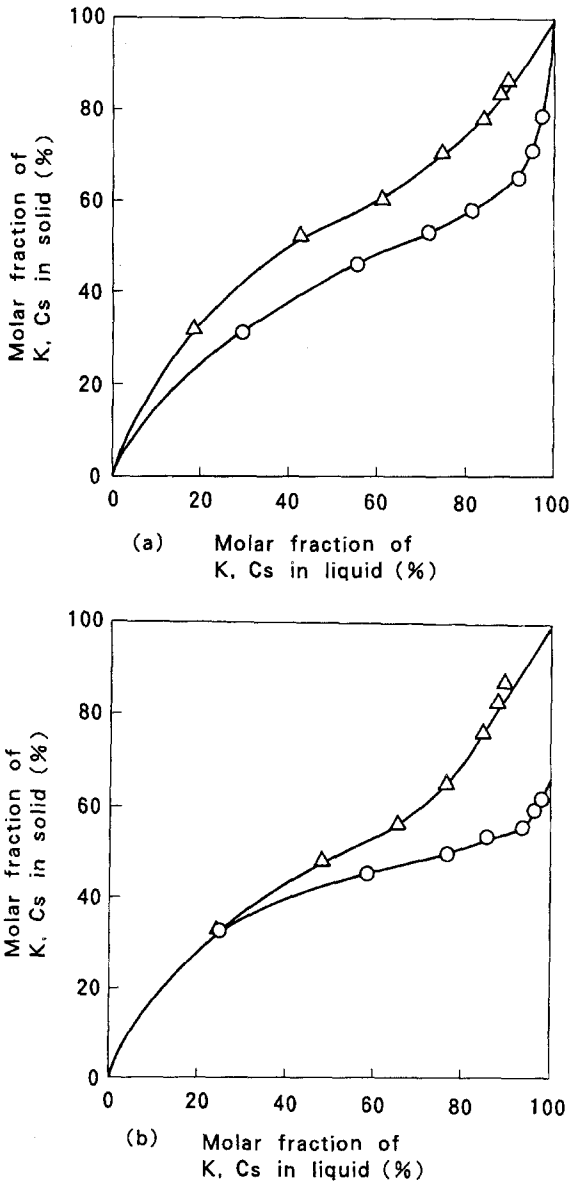

Figure 4 Ion-exchange isotherms of Cs/K with Na–X (b) and the precursor (a) at 298 K; ○, Cs; △, K.

superimposed together, signifying reversible adsorption/desorption of water.

The TG curves for zeolite precursors dried at 373 K (solid lines in Fig. 5a and c) were rather similar to those of well-crystallized zeolites (Fig. 5b and d), while samples preheated at 723 K (broken lines in Fig. 5a and c) showed essentially no change in the weight. The weight loss given by solid lines in Fig. 5a and c were presumably due to dehydration of terminal OH in the precursor, such as a sodalite unit. A sample preheated at 723 K has finished the structural dehydration and retains no available site for water adsorption on exposure to moist air. Thus the dehydrative linkage of the structural unit (sodalite unit) in the precursor may occur thermally, but a hydrothermal reaction is essential to build up the zeolite framework.

3.5. ^{29}Si and ^{27}Al MAS NMR

Fig. 6 shows ^{29}Si MAS NMR spectra for Na–X, Na–A zeolite and their amorphous precursors. The spectrum of crystalline Na–X zeolite (Si/Al = 1.45) showed five

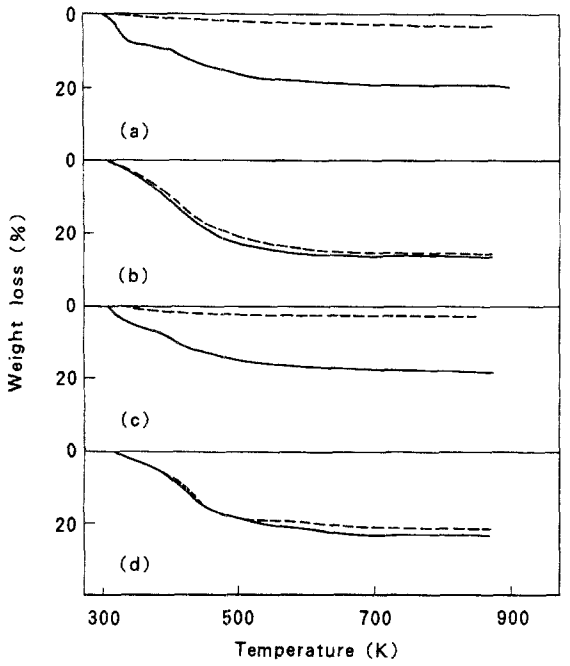

Figure 5 TG curves for Na–X (b), Na–A zeolite (d) and their amorphous precursors ((a) for Na–X, (c) for Na–A) after exposure to moist air: solid lines, dried at 373 K; broken lines, heated at 723 K.

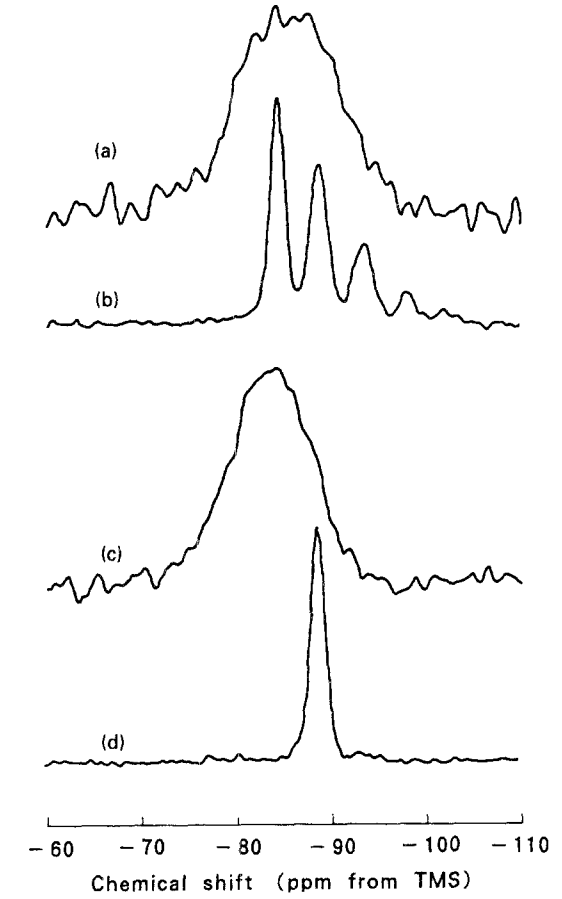

Figure 6 ^{29}Si MAS NMR spectra for Na–X (b), Na–A zeolite (d) and their amorphous precursors ((a) for Na–X, (c) for Na–A).

signals at −84.3, −88.7, −93.5, −97.9 and −101.8 ppm (Fig. 6, curve b) with decreasing intensity in this order, in good agreement with that reported for Na–X with Si/Al = 1.35 [16], of which peaks should be assigned to $Si(OAl)_4$, $Si(OAl)_3(OSi)$, $Si(OAl)_2(OSi)_2$, $Si(OAl)(OSi)_3$ and $Si(OSi)_4$, respectively. In contrast, the spectrum for the amorphous precursor for Na–X showed a single, broad signal at *c.* −85 ppm (Fig. 6, curve a). In the crystallization of Na–A, a shift from −84.3 to −88.8 ppm with sharpening of the peak was observed in ^{29}Si NMR spectra (Fig. 6, curves c and d), as reported in the literature [17]. The sharp peak at −88.8 ppm (Fig. 6, curve d) for Na–A zeolite was assigned to $Si(OAl)_4$.

In the spectra of ^{27}Al MAS NMR given in Fig. 7, on the other hand, a strong peak of tetrahedral Al at *c.* 58 ppm was observed for every sample of Na–X (curve b), Na–A (curve d) zeolite and their amorphous precursors (curves a and c) and was assigned [17, 18] to $Al(OSi)_4$ following the Loewenstein's law [19] to prohibit Al–O–Al bond. Sharpening of the ^{27}Al peak was again observed after crystallization of both zeolite Na–X and Na–A.

It is well known that chemical shift in ^{29}Si MAS NMR spectra for many silicate compounds [20, 21] and zeolites [22] is dependent on the mean distance of the Si–O bond and/or mean angle of Si–O–T. Thus the broadening in ^{29}Si (Fig. 6a and c) and ^{27}Al (Fig. 7, curves a and c) NMR peaks for both precursors might be interpreted as the formation of Si–O–T bonds with a wide distribution of distance and angle in the induction period for Na–X and Na–A synthesis. The simultaneous sharpening of ^{29}Si (Fig. 6) and ^{27}Al (Fig. 7) peaks during crystallization of the zeolite suggests that flexible Si–O–T bonds in the amorphous

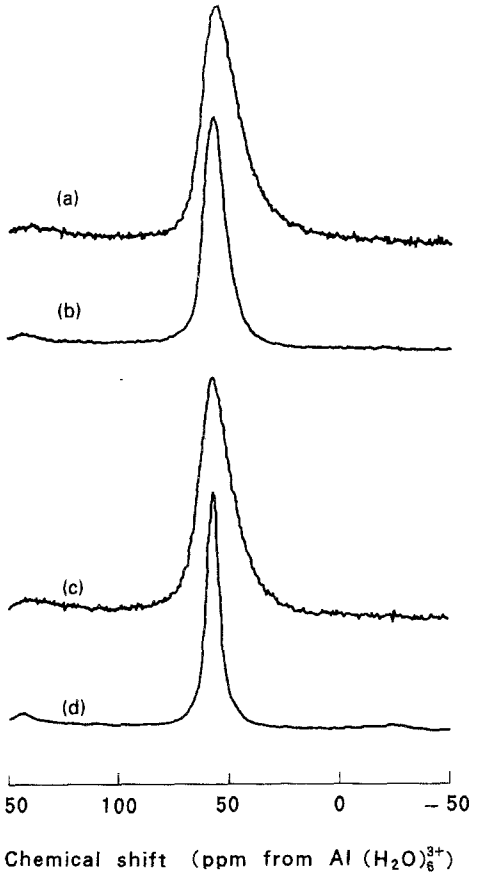

Figure 7 ^{27}Al MAS NMR spectra for Na–X (b), Na–A zeolite (d) and their amorphous precursors ((a) for Na–X, (c) for Na–A).

precursor are transformed into rigid bonds with a distinct coordination number in the well-crystallized zeolite. The suggestion was strongly supported by the fact that similar sharpening of peaks was observed in IR spectra, as mentioned above.

Application of solid-state MAS NMR to fly ash zeolite was unfavourable because of contamination with magnetite (Fe_3O_4) included in fly ash as a raw material [4, 23], and therefore was not carried out in the present work.

3.6. XPS-AES chemical state plots of Si and Al for zeolites

Two-dimensional plot of photoelectron binding energy and Auger kinetic energy permits a more accurate description of the chemical state [24, 25]. The plots of Si and Al for a series of aluminosilicate zeolites are correlated on a single line, but simple oxides and non-zeolite minerals lie on a different line [8, 24, 25].

Figs 8 and 9 show the chemical state plots of Si and Al, respectively, for Na–X, Na–A, fly ash zeolite and their amorphous precursors, where data for Na–Pl, Na–Y zeolite and hydroxy-sodalite are also indicated for reference. In these figures, zeolites and the precursors were correlated on a single line, showing that the precursors were classified as a quasi-zeolite. Some disagreement between authentic and fly ash zeolite was observed, presumably arising from that fly ash zeolite was composed of zeolite and non-zeolitic sodium aluminosilicate [4]. It is of interest to note that in Figs 8 and 9, the plots of precursor for authentic Na–X and Na–A zeolites are rather close together, while the corresponding zeolites lie apart from each other. It seems likely that chemical states of Si or Al are in a similar environment (sodalite unit) among the precursors formed in the induction period, and then the different characteristic of each zeolite species appears on building-up the crystalline framework.

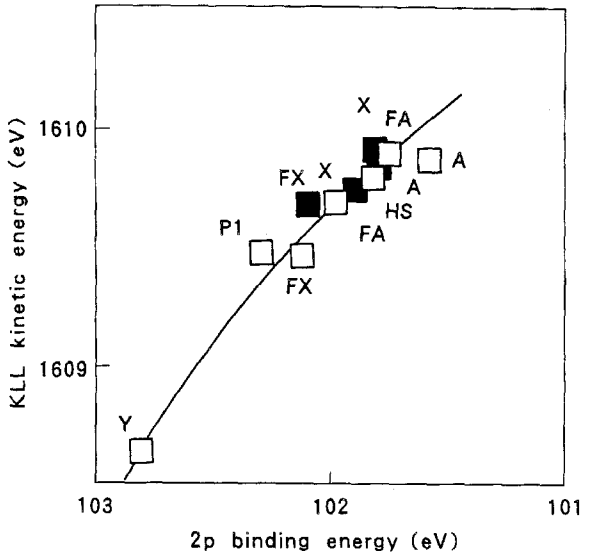

Figure 8 Si chemical state plots for Na-zeolites (□) and their precursors (■); HS, hydroxysodalite; FA, Na–A from fly ash; FX, Na–X from fly ash.

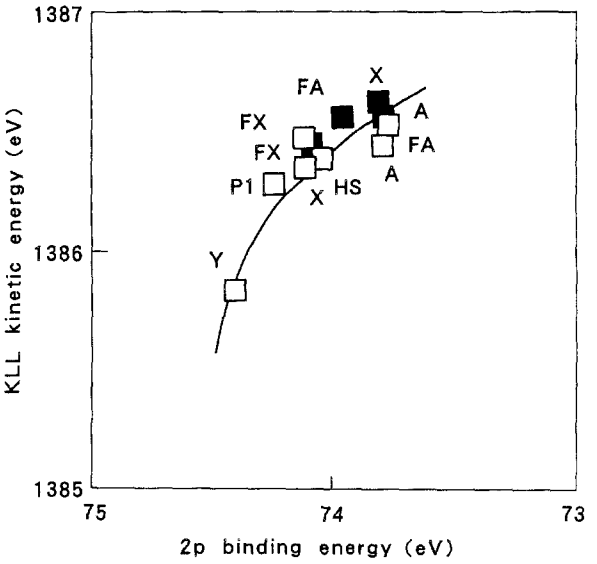

Figure 9 Al chemical state plots for Na-zeolites (□) and their precursors (■); symbols as in Fig. 8.

4. Conclusion

An amorphous precursor with a composition close to the target zeolite was formed during the induction period of a hydrothermal reaction for Na–X and Na–A zeolites. The IR spectra revealed that a structural unit with terminal OH was formed in the induction period, and then coupled together through dehydration of terminal OH to build up the zeolite framework of Na–X or Na–A. By comparative Cs/K ion-exchange studies, the formation of D6R external linkage was confirmed in crystallization of Na–X zeolite.

Comparing ^{29}Si or ^{27}Al MAS NMR spectra between zeolites and their amorphous precursors, the transformation from flexible to rigid Si–O–T bond was suggested in the crystallization process of Na–X and Na–A zeolites.

The IR spectra and XPS/AES chemical state plots of Si and Al for both fly ash zeolites and their amorphous percursors were compatible with those for authentic Na–X and Na–A zeolites and their precursors, respectively.

References

1. R. D. SMITH, *Prog. Energy Combust. Sci.* **6** (1980) 53.
2. G. L. FISHER, D. P. T. CHANG and M. BRUMMER, *Science* **192** (1976) 553.
3. N. SHIGEMOTO, K. SHIRAKAMI, S. HIRANO and H. HAYASHI, *Nippon Kagaku Kaishi* **1992** (1992) 484.
4. N. SHIGEMOTO, K. MIYAURA and H. HAYASHI, *J. Mater. Sci.* **28** (1993) 4781.
5. N. SHIGEMOTO, K. MIYAURA, S. SUGIYAMA and H. HAYASHI, *J. Mater. Sci. Lett.*, **13** (1994) 660.
6. E. F. FREUND, *J. Cryst. Growth* **34** (1972) 11.
7. H. C. HU, W. H. CHEN and T. Y. LEE, *ibid.* **108** (1991) 561.
8. A. M. WINIECKI, S. L. SUIB and M. L. OCCELLI, *Langmuir* **4** (1988) 512.
9. E. M. FLANIGEN, H. KHATAMI and H. A. SZYMANSKI, *Adv. Chem. Ser.* **101** (1971) 201.
10. M. DECOTTIGNIES, J. PHALIPPOU and J. ZARZYCKI, *J. Mater. Sci.* **13** (1978) 2605.
11. A. BERTOLUZZA, C. FAGNANO, M. A. MORELLI, V. GOTTARDI and M. GUGLIELMI, *J. Non-Cryst. Solids* **48** (1982) 117.

12. S. R. STOJKOVIC and B. ADNADJEVIC, *Zeolites* **8** (1988) 523.
13. H. S. SHERRY, *J. Phys. Chem.* **70** (1966) 1158.
14. R. M. BARRER, L. V. C. REES and M. SHAMSUZZOHA, *J. Inorg. Nucl. Chem.* **28** (1966) 629.
15. R. M. BARRER, J. A. DAVIES and L. V. C. REES, *ibid.* **31** (1969) 2599.
16. J. KLINOWSKI, S. RAMDAS, J. M. THOMAS, C. A. FUFE and S. HARTMAN, *J. Chem. Soc. Faraday Trans. 2* **78** (1982) 1025.
17. G. ENGELHARDT, B. FAHLKE, M. MAGI and E. LIPPMAA, *Zeolites* **3** (1983) 292.
18. C. A. FUFE, G. C. GOBBI, J. S. HARTMAN, J. KLINOWSKI and J. M. THOMAS, *J. Phys. Chem.* **86** (1982) 1247.
19. W. LOEWENSTEIN, *Amer. Mineral* **39** (1954) 92.
20. J. V. SMITH and C. S. BLACKWELL, *Nature (London)* **303** (1983) 223.
21. J. V. SMITH, C. S. BLACKWELL and G. L. HOVIS, *ibid.* **309** (1984) 140.
22. J. KLINOWSKI, *Prog. NMR Spectrosc.* **16** (1984) 237.
23. S. C. WHITE and E. D. CASE, *J. Mater. Sci.* **25** (1990) 5215.
24. C. D. WAGNER, H. A. SIX, W. T. JANSEN and J. A. TAYLOR, *Appl. Surface Sci.* **9** (1981) 203.
25. C. D. WAGNER, D. E. PASSOJA, H. F. HILLERY, T. G. KINISKI, H. A. SIX, W. T. JANSEN and J. A. TAYLOR, *J. Vac. Sci. Technol.* **21** (1982) 933.

Received 8 March 1994
and accepted 8 June 1995